D. Trache, F. Maggi, I. Palmucci, L.T. De Luca
Thermal Behavior and Decomposition Kinetics of Composite Solid Propellants in the Presence of Amide Burning Rate Suppressants
Journal of Thermal Analysis and Calorimetry, Vol. 132, N. 3, 2018, p. 1601-1615
doi:10.1007/s10973-018-7160-8

Thermal behavior and decomposition kinetics of composite solid propellants in presence of amide burning rate suppressants

Djalal Trache[a,*], Filippo Maggi[b], Ilaria Palmucci[b], Luigi T. DeLuca[b]

[a] *UER Procédés Energétiques, Ecole Militaire Polytechnique, BP 17, Bordj-el-Bahri, 16111, Algiers, Algeria.*

[b] *SPLab, Dept. of Aerospace Science and Technology, Politecnico di Milano, 34 Via La Masa, 20158Milan, Italy.*

* Corresponding author: Tel: +213 661808275, Fax: +213 21863204

Abstract

The employment of burning rate suppressants in the solid rocket propellant formulation is long known. Different research activities have been conducted to well understand the mechanism of suppression, but literature about the action of oxamide (OXA) and azodicarbonamide (ADA) on the thermal decomposition of composite propellant is still scarce. The focus of this study is on investigating the effect of burning rate suppressants on the thermal behavior and decomposition kinetics of composite solid propellants. Thermogravimetric analysis (TG) and differential thermal analysis (DTA) have been used to identify the changes in the thermal and kinetic behavior of coolant-based propellants. Two main decomposition stages were observed. It was found that OXA played an inhibition effect on both stages, whereas the ADA acts as a catalyst in the first stage and as coolant in the second one. The activation energy dependent on the conversion rate was estimated by two model-free integral methods: Kissinger-Akahira-Sunose (KAS) and Flynn-Wall-Ozawa (FWO) based on the TG data obtained at different heating rates. The mechanism of action of coolants on the decomposition of solid propellants was confirmed by the kinetic investigation as well.

Keywords: burning rate suppressant, composite propellant, thermal analysis, decomposition kinetics, iso-conversional model.

1. Introduction

Composite solid propellants find application in defense technology (*e.g.* rockets and missiles) as well as space exploration (*e.g.* strap-on boosters and space launchers) and have been used in propulsion systems for several decades [1-3]. Composite propellants are mainly made up of some inorganic oxidizers such as ammonium perchlorate (AP) and ammonium dinitramide (ADN), polymeric binders such as hydroxyl-terminated polybutadiene (HTPB) and glycidyl azide polymer (GAP), a metal fuel such as aluminum (Al), additives such as curing agents, fillers, burning rate modifiers (catalyst or coolant), plasticizers, stabilizers and other components [4-7]. The AP/HTPB/Al-based propellants present excellent burning and mechanical features, acceptable cost, processability and storability, and are considered by far the most mature propulsion system among those currently employed [1, 8].

Additives are commonly incorporated to propellant formulations in small amount to tailor ballistic properties and improve peculiar propellant characteristics at the expense of other parameters, looking for a compromise among properties. Ballistic modifiers are substances that can be added in few percent ratios (between 0.5% and 3% of the oxidizer) in order to enhance (for catalysts)/reduce (for coolants) the burning rate or diminish its sensitivity to initial temperature or pressure in a controlled way [8-11]. Composite solid propellants with high burning rate are often requested in high performance rocket motors and would allow vehicles to fly at high speeds (for instance: rockets and missiles). On the other hand, propellants with low burning rate produce low thrust, and are utilized for example as a slow burning rocket booster or a gas generator for controlling vehicle flight [12-14].

A convenient propellant formulation should have stable burning rate and a low pressure exponent [8]. To accomplish this purpose, substantial efforts have been devoted, including the incorporation of coolants into propellant formulations. A number of coolants, usually referred to as burning rate suppressants, have been investigated such as strontium carbonate, triphenyl antimony, ammonium polyphosphate, ammonium chloride, lithium fluoride, hexabromocyclododecane and diammonium bitetrazole [15, 16]. Further inorganic salts such as sodium carbonate, sodium bicarbonate calcium carbonate have demonstrated acceptable burning rate retarding effects [16]. Various explosives such as 3-amino-5-1,2,4-triazole, 3-nitro-1,2,4-trazol-5-one, nitroguanidine and triaminotrinitrobenzene have been reported as coolants [16-18]. Other prospective burning rate suppressants including diaminoglyoxime, diaminofurazan, biuret, urea, melamine, oxamide and azodicarbonamide have been extensively studied as well [8, 12, 19-22]. Amide-based compounds are considered as the most effective and are frequently employed as coolants in practical use of composite propellants.

The decomposition characteristics and the kinetics behavior of composite solid propellants exert a profound influence on the combustion features, since the decomposition is considered as the initial stage of combustion [23]. Thermal analysis investigation of energetic materials such as solid propellants is crucial not only to understand the kinetics of their thermal decomposition but also to deeply evaluate the effect of their exothermic decomposition on the potential hazard in their handling, processing, storage, and use [24-27]. Kinetic studies provide useful information to aid the modeling and prediction of the combustion characteristics of solid rocket propellants as well [28-30]. Non-isothermal kinetics can be categorized into model-free and model-fitting classes [31-33]. Both methods have their benefits. They are

77 complementary rather than in competitive between each other. Recently, it was
78 demonstrated that model-free methods, also known as iso-conversional methods, are
79 the most common employed methods in the kinetic study of decomposition of
80 energetic materials [34, 35]. The “International Confederation for Thermal Analysis
81 and Calorimetry (ICTAC)” committee recommended that utilizing multiple heating
82 rate programs leads to more reliable kinetic parameters with respect to single heating
83 rate program [36]. Usually, the thermoanalytical methods employed for the study of
84 thermal decomposition and kinetics of energetic materials (like propellants and
85 propellant ingredients) are thermogravimetric analysis (TG), differential thermal
86 analysis (DTA) and differential scanning calorimeter (DSC) [37-41]. Recently, these
87 techniques have been revealed to be requisite to assess the effect of ballistic modifiers
88 on the thermal decomposition and kinetic parameters of solid propellant [39, 42-44].
89 Commonly, several parameters are needed to be evaluated, including decomposition
90 temperature, heat of decomposition, activation energy, pre-exponential factor,
91 reaction model as well as thermolysis chemical pathway [23, 45, 46]. At present, the
92 behavior of various catalysts as ballistic modifiers in the thermal decomposition of
93 AP-based propellant has been extensively studied [23, 47-49]. Nevertheless, only few
94 studies dealing with the effect of burning rate suppressants on the thermal properties
95 of solid propellants have been carried out [12, 16, 19, 20]. Furthermore, to the best of
96 our knowledge, there was no available report describing the influence of amides based
97 compounds (oxamide and azodicarbonamide) on the thermal decomposition of
98 composite solid propellants. Our previous research found that OXA and ADA are
99 acting on both condensed and gas phases during combustion and the nature of coolant
100 affects differently the burning rate pressure index [8].

The purpose of this paper is to systematically investigate the effect of amide based compounds on the thermal decomposition characteristics of composite propellant formulations. This study first focused on the evaluation of the thermal properties of composite propellants containing two different coolants at different ratios based on TG-DTA technique using multi-heating rate method to well understand the role of coolants. Then, two model free integral methods (Flynn–Wall–Ozawa (FWO) and Kissinger–Akahira–Sunose (KAS) methods) were used to compute the activation energy describing the thermal decomposition mechanism of composite solid propellants. An attempt has been made to explain the observed mechanisms that govern the functioning of cooling agents during propellants decomposition.

2. Materials and methods

2.1. Materials

Bimodal ammonium perchlorate (AP), coarse AP (cAP) and fine AP (fAP), was employed as oxidizer in this work. The cAP with mean particles diameter of 200 μm was procured from a propulsion supplier and fAP, prepared by milling utilizing a centrifuge grinder (Restsch S100), has a mean diameter of 10 μm as determined by Malvern Mastersizer 2000 analyzer. The metal powder, which was used as a high-energy fuel, is a commercial spherical μAl (of spherical shape with 30 μm nominal diameter). Hydroxyl-terminated polybutadiene (HTPB), a polyfunctional oligomer of butadiene which comes with hydroxyl groups, was procured from Cray Valley. Dioctyl adipate (DOA), isophorone di-isocyanate (IPDI) used respectively as plasticizer and curing agent were provided from Acros-Carlo Erba and Alfa Aesar, respectively. Dibutyltin diacetate (TIN) and oxamide (OXA) were employed as curing catalyst and ballistic modifier, respectively, and were supplied by Sigma Aldrich.

126 Azodicarbonamide (ADA) used also as a ballistic modifier was procured from Acros
127 Organics. All the compounds were used as received.

128 *2.2. Preparation of propellant samples*

129 HTPB and other liquid ingredients (except curing agent) were well mixed and
130 degased. The propellant was cured using isocyanate and tin-based catalyst. The
131 baseline propellant AP/Al/HTPB formulated in the present study encompasses 86
132 mass % total-solids with 58 wt.% cAP and 10 wt.% fAP. In the case of propellant
133 formulations comprising OXA or ADA, the coolant is used in replacement of cAP
134 particles, so that the grand total of mass-based solid loading and the fAP/HTPB ratio
135 are the same as in the corresponding baseline. All the propellant formulations details
136 are summarized in Table 1.

137 The propellant ingredients were weighted with <0.5% error. All propellant
138 mixtures were produced in 100 g batches using a Resodyn LabRAM resonant mixer.
139 Air bubbles trapped in the propellant slurry while mixing were removed by degassing
140 in a vacuum-casting chamber. The mixed slurry was subsequently pressed into Teflon
141 molds, cured initially at 36 °C for 24 h, and followed by another curing at 60 °C for
142 48 h. The obtained samples have been used for evaluation of the thermal properties
143 and kinetics.

144 *2.3. TG-DTA analysis*

145 Thermal decomposition experiments of the propellant samples were carried out
146 using a simultaneous TG-DTA analyser (Seiko Hitachi model SII Exstar 6000). The
147 instrument was calibrated against melting point of indium, tin, lead, zinc and silver. In
148 all experiments, 1–3 mg of propellant was placed in an alumina open crucible. The
149 temperature was raised from room temperature to 900 °C. Argon gas atmosphere
150 (high-purity) at a flow rate of 100 ml min^{-1} was used as the purge gas. The non-

isothermal TG-DTA runs were conducted at heating rates (β) of 5, 10, 15, 20 and 25 °C min^{-1}. Data acquisition and processing were done with Muse version 2.0 software. Each test was repeated at least two times and the repeatability of the data is good, demonstrating the efficiency of the mixing procedure and the homogeneity of the prepared composite samples.

2.4. Kinetic modeling

2.4.1. The basis of non-isothermal kinetic model

The rate of many thermally stimulated processes can be usually written in terms of T and α as follow [36, 34]:

$$\frac{d\alpha}{dt} = k(T) f(\alpha) \quad (1)$$

where t is the time, T is the temperature in Kelvin, α is the conversion extent ($0<\alpha<1$), $k(T)$ is the rate constant and $f(\alpha)$ is the mathematical function that represents the reaction mechanism. The value of α is experimentally derived from the thermal analysis technique used as a fraction change of any physical property associated with the reaction progress. When the process progress is monitored as a change in mass by TG, α is computed as a ratio of the current mass change, Δm, to the total mass change, Δm_{tot}, occurred throughout the process:

$$\alpha = \frac{m_0 - m_t}{m_0 - m_\infty} \quad (2)$$

where m_0, m_t and m_∞ are initial sample mass, sample mass at time t and sample mass at the end of reaction, respectively.

The temperature dependence of $k(T)$ can be satisfactory described by the Arrhenius law, which after substitution into Eq. (1) yields,

$$\frac{d\alpha}{dt} = A \exp(-E/RT) f(\alpha) \quad (3)$$

where A is the pre-exponential factor (in s^{-1}), E the activation energy and R the universal gas constant.

When heating rate $\beta=dT/dt$ is introduced, Eq. (3) could be transformed to:

$$\frac{d\alpha}{dT}=\frac{A}{\beta}\exp(-E/RT)f(\alpha) \quad (4)$$

Integration of Eq. (4) leads to

$$g(\alpha)=\int_0^{\alpha}\frac{d\alpha}{f(\alpha)}=\frac{A}{\beta}\int_{T_0}^{T}\exp(-E/RT)dT \quad (5)$$

where $g(\alpha)$ is the integral form of the reaction model $f(\alpha)$.

Integral methods originate from the application of the iso-conversional principle to Eq. (5). The integral in this equation does not have an analytical solution for an arbitrary temperature program. Numerous approximate equations have been proposed in the literature to perform the kinetic analysis of solid-state reactions. The most popular are those suggested by Doyle [50], Coats-Redfern [51, 52] and Senum and Yang [53].

2.4.2. Model free integral methods

Previous research works reported that iso-conversional methods can be utilized to compute activation energy (E) without considering the reaction mechanism. In this paper, Kissinger–Akahira–Sunose (KAS) and Flynn-Wall-Ozawa (FWO) methods have been employed to evaluate the activation energies of propellant samples during thermal decomposition, because of their good adaptability and validity for model-free approaches [54]. The KAS and FWO are defined in Eqs. (6) and (7), respectively.

$$\ln\left(\frac{\beta}{T_\alpha^2}\right)=\ln\left[\frac{AR}{g(\alpha)E}\right]-\frac{E}{RT_\alpha} \quad (6)$$

$$\ln\beta=\ln\left[\frac{0.0048AE}{g(\alpha)R}\right]-1.0516\frac{E}{RT_\alpha} \quad (7)$$

196 At a constant value of conversion rate α, the plots of $\ln(\beta/T_\alpha^2)$ vs. $1/T_\alpha$ (TAS
197 method) or ln β vs. $1/T_\alpha$ (FWO method) obtained from thermograms recorded at
198 several heating rate help in yielding a straight line whose slope allows evaluation of
199 the apparent activation energy.

200 **3. Results and Discussion**

201 *3.1. TG-DTA analysis of propellant samples*

202 The TG-DTA analyses of the different samples shown in Figs. 1 and 2 indicate
203 three major reaction stages in the temperature range 160–600 °C. The different stages
204 appeared as steps in TG and as endothermic/exothermic peaks in DTA. On reaching
205 600 °C all the propellant samples lose ~80% of the initial mass, there was no
206 significant mass loss or thermal event occurred up to 900 °C and hence the data
207 beyond 600 °C are excluded from the investigation.

208 *3.1.1. Thermal decomposition features of the baseline formulation*

209 The non-isothermal TG and DTG curves of the control propellant (CP-Baseline)
210 are shown in Figs. 1 (a) and (b). It can be seen that CP-Baseline exhibited apparently
211 three decomposition stages. The early mass loss at around 210 °C could be due to the
212 evaporation or decomposition of the plasticizer (DOA) [47, 55]. The two other stages
213 were observed as steps of mass loss in TG. The first major decomposition stage (stage
214 II) occurred in the temperature range 300–410 °C, while the second decomposition
215 happened in the temperature range of 430–520 °C (stage III). The mass loss pattern
216 observed for the CP-Baseline is a typical thermal response of composite solid
217 propellants containing AP as oxidizer and HTPB as binder [56].

218 Studying the DTG curve of CP-Baseline, two overlapping peaks are observed
219 (Fig. 1(c)). The overlapping peaks produce a single DTG peak with a shoulder located
220 on the left. CP-Baseline underwent two complicated decomposition processes at this

stage, a low-temperature decomposition (LTD, <360 °C) and a high-temperature decomposition (HTD, >360 °C). DTG of CP-Baseline exhibited basic features of AP decomposition suggesting its predominant role, but a little change can be observed in that stage II, since well-resolved peaks are commonly obtained in the case of AP/AP-propellant decomposition [35, 49, 57]. This difference is probably caused by the presence of micro-aluminum. It is worth noting that one of the most important decomposition mechanisms of AP is that of proton transfer, where LTD is considered to start from cation to anion via molecular complex and occurred mainly at the intersections of dislocations in the bulk crystals. It generates in pores beneath the surface at a distance of few microns [49]. Zhu et al. [58] demonstrated that the presence of an amount of Al was likely to adsorb onto the surface of AP causing the inhibition of its sublimation and dissociation process and leading to the increase of the first decomposition process (LTD), whereas a decrease of HTD occurred. This latter can be catalyzed by Al, which is an active metal with high reactivity, that can react easily with the decomposition products of AP. However, the amount of Al involved in these reactions is probably small, since most of Al reacts at higher temperature [59]. During this stage II the CP-Baseline loses ~80% of its mass, since the process involves the thermal decomposition of all AP as well as a part of the binder. Wang et al. reported that thermal decomposition process of AP and HTPB accelerates during this stage, a large amount of heat is released and many kinds of oxidizing gases are formed [56]. However, as shown in Fig. 1(d), an additional decomposition of the residual polymeric binder occurs at higher temperature (~450°C) [35]. This latter phenomenon is governed by a diffusion process [55].

The DTA curve of CP-Baseline (Fig.2) indicates that its thermal behavior consists of three stages. In the stage Ib, an endothermic peak appears at 245 °C,

without mass loss, which is ascribed to the endothermic crystallographic transition of AP from orthorhombic to cubic due to the rotation of the perchlorate ion [57]. In the subsequent two stages, the first main exothermic peak (stage II) appears in the temperature range 280–420 °C corresponding to the complete decomposition of AP with a part of the polymeric binder, while the second peak (stage III) appears at relatively higher temperature range 430–550 °C, indicating the exothermic decomposition of the residual binder. Al-Basuony et al. [60] reported that composite propellant binders based on HTPB decompose in two stages. The first exothermic stage from 300-400 °C is divided into three sub-steps which are (1) an endothermic depolymerization of the binder through urethane bond cleavage that causes the diisocyanate component to vaporize, (2) exothermic cyclization and (3) cross-linking of the remaining HTPB, accompanied by partial decomposition of the cyclized products into low molecular mass species that volatize at around 350 °C. The second stage is attributed to the decomposition of the cyclized and cross-linked products formed in the first stage. Furthermore, some earlier reports for AP-based propellants also showed the appearance of one main exothermic peak, which combines both LTD and HTD [29, 61], in stage II corroborating our findings.

3.1.2. Effect of OXA on the thermal decomposition characteristics of propellants

The thermogravimetric analyses of the propellant samples with two different amount of OXA were carried out and the TG curves obtained are shown in Fig. 1(a). The results indicate that the OXA-based propellants exhibit a three-stage decomposition. These decomposition patterns of propellants with the addition of OXA show notable differences with respect to the control propellant.

Figure 1(b) displays the DTG curves of CP-Baseline and propellants in the presence of two different amounts of OXA. The first peak (stage Ia) corresponds to

271 the decomposition of OXA, where the surface of the peak increases with the increase
272 of the amount of OXA, and to the evaporation of DOA. Our previous work
273 demonstrated that this decomposition is an endothermic phenomenon following a
274 two-step process and the main decomposition product is NH_3 [8]. The addition of 0.5
275 wt.% and 3 wt.% of OXA increased the main decomposition temperature of
276 propellant (stage II) by 6.5 °C and 8.6 °C at a burning rate of 5 °C min^{-1}, respectively.
277 The incorporation of OXA, which decomposes at lower temperature, to the propellant
278 samples inhibits the decomposition processes. The abundance of NH_3 causes
279 suppression of the oxidizer sublimation and dissociation and shifts the chemical
280 balance of the AP decomposition to left, so that both condensed gas-phase reactions
281 occurred in the propellant surface are decelerated. The HTD of AP belongs to gas
282 phase reaction. It is known that the thermolysis of OXA is highly endothermic. The
283 decomposition products of such as CO and NH_3 enable the concentration of $HClO_4$ to
284 become dilute and carry away the heat from the gas phase, thus the peak temperature
285 for HTD of AP is also raised. Accordingly, as the amount of OXA increased, the main
286 exothermic peak (stage II) that was attributed to the complete decomposition of AP
287 and a part of binder gradually shifted toward higher temperature. It was shown from
288 Fig. I(c) that LTD is shifted to the higher temperature and merged with the HTD,
289 displaying one pronounced peak of decomposition.

290 The second decomposition of OXA-propellants, corresponding to the
291 decomposition of the residual binder, follows the same trend as the first one. The
292 DTG values related to this decomposition (stage III) are 441.6, 449.2 and 452.0 °C for
293 CP-Baseline, CP-OXA1 and CP-OXA2 at a burning rate of 5 °C min^{-1}, respectively.
294 These findings can be explained by the inhibition action of the decomposition process
295 in the condensed-phase and the important volume of inert diluents such as N_2

296 reaching the gas-phase. Therefore, the flame temperature will decrease and
297 subsequently affects the heat feedback to the propellant surface. Diffusion controlled
298 combustion dominates and this justifies the lower pressure exponent of OXA-based
299 propellants, as reported in our recent published work [8].

300 When the DTA data were analyzed (Fig.2), two main peaks were observed in the
301 range of 250–520 °C. Once OXA is added to the propellant formulations, similar
302 trend has been obtained with respect to TGA. Furthermore, during heating, at around
303 245 °C, the orthorhombic lattice of AP expands and forms a cubic structure which is
304 invariably observed in all the samples as an endothermic peak in the DTA curves.

305 Our results matched well with those obtained by an effective burning rate
306 suppressant *vis.* Ammonium oxalate where the thermal decomposition of AP-based
307 composite propellant is restrained and shifted to higher temperature (~6.8 °C) and
308 consequently the combustion behavior is sensibly affected [44].

309 *3.1.3. Effect of ADA on the thermal decomposition characteristics of propellants*

310 To compare the influence of ADA on the thermal decomposition of composite
311 propellants, thermogravimetric analyses have been performed and the TG profiles
312 obtained are given in Fig. 1 (a). It is shown that the thermal decomposition process
313 could be divided into three main stages. The thermal analysis curves obviously
314 displayed the change in peak temperature of the decomposition stages II and III of the
315 propellant samples with respect to the amount of ADA.

316 To well understand the various decomposition stages of samples, the DTG curves
317 shown in Fig. 1(b) were plotted by taking the first derivative of the TG data. Similarly
318 to TG, DTG exhibited three different stages. The stage Ia occurred from 150–250 °C
319 is due to the early decomposition of ADA, where the surface of the peak increases
320 with the increase of the amount of ADA, and to the evaporation of DOA. Our

previous work revealed that this decomposition is mainly an exothermic phenomenon with the formation of low molecular weight gases H_2, CO, N_2 and cyanic acid [8]. This exothermicity could promote the decomposition of AP particles and might enhance the regression rates of AP by reducing its decomposition temperature. The addition of 0.5 wt.% and 3 wt.% of ADA decreased the main decomposition temperature of propellant (stage II) by 7.9 °C and 18.7 °C at a burning rate of 5 °C min^{-1}, respectively. It can be seen from Fig .1 (c) that ADA significantly accelerates the high-temperature exothermic process of AP, which the main ingredient of the solid propellant on one hand. On the other hand the decomposition of the binder is promoted owing to the important heat feedback. It is believed however that this behavior is a result of the greater influence of kinetics that likely occurs between the oxidant species and the fuel vapors burning relatively close to the surface. We can deduce from the above discussion that ADA plays initially a catalytic effect. The last stage (III) takes place at temperature above 430 °C as shown in Fig. 1(d), with little mass loss, mainly dominated by the decomposition of the residual binder. The DTG values related to this decomposition (stage III) are 441.6, 448.0 and 451.1 °C for CP-Baseline, CP-ADA1 and CP-ADA2 at a burning rate of 5 °C min^{-1}, respectively. It can be observed that the complete decomposition of ADA, generating an important volume of inert diluents such as N_2, could possibly change the composition of reactants reaching the gas-phase and causes the decrease of the flame temperature. These gases can significantly inhibit the heat flow from the gaseous combustion zone back to the condensed phase and thus slow down the thermal decomposition of the residual polymeric binder. Furthermore, fuel vapors have to travel a large distance in order to get oxidized and diffusion becomes dominant, since important volume of

inert gases is released by ADA. More inert gases can be released by CP-ADA2compared to CP-ADA1.

The thermogravimetric analysis data were supported by DTA results, where two main decomposition peaks were observed in the range of 250–520 °C. Further, the exothermecity of ADA in CP-ADA2 is perceptible from Fig. 2 at around 230 °C, whereas no peak appeared for CP-ADA1 at this stage (Ia), probably because of the low amount of ADA in the formulation. It was observed that the endothermic transformation happens from the low-temperature orthorhombic phase to the high-temperature cubic phase in the range 240–250 °C (stage Ib) is not affected by the incorporation of ADA.

3.2.Kinetic analysis

The purpose of thermal decomposition experiment was to gain kinetic parameters including the activation energy to predict the thermal decomposition process. Because all high-energy materials are not thermodynamically stable, their existence is made possible by kinetic factors. Therefore, kinetic parameters are important for the prediction of the safety and efficiency of AP-based propellants and allow understanding the role of different additives such as ballistic modifiers.

3.2.1. Effect of heating rate

In order to use multi-heating rate method, a series of experiments had to be conducted at various heating rate (5, 10, 15, 20 and 25 °C min^{-1}), and the TG/DTG curves of CP-OXA1 were shown in Fig. 3. The different results of TG for different propellant samples were listed in Table 2. Firstly, for the two decomposition processes of the propellant samples, both points of maximum of mass loss rate in the TG and DTG curves shifted toward higher temperatures. This could be attributed to difference between the reference temperature and sample temperature due to heat and

mass transfer limitation. Further, the low thermal conductivity of propellant samples also caused temperature gradients in sample grains. This is because thermal conductivity of a composite material depends on that of the composite material ingredients as stated by Gaurav and Tamakrishma [62]. As HTPB has very low thermal conductivity 2.01 W m^{-1} K^{-1} [63] compared to that of aluminum which is 206 W m^{-1} K^{-1} [62], 14 wt.% of HTPB decreases the thermal conductivity of propellant samples. Consequently, the temperature in the core of grains can be lower than the temperature on their surfaces. Secondly, the percentage of mass losses is about 70% and 5% for both decomposition steps, respectively. It can be trusted that heating rate could not affect residues yield obviously. On the other hand, Fig. 4 illustrated the DTA patterns of the exothermic decomposition of CP-OXA1 at different heating rate. It showed a similar trend as the TG analysis. Furthermore, it was found that the allotropic transition at around 245 °C did not affected by the heating rate.

3.2.2. Analysis of the activation energy

Figures 5and 6 display the plots of iso-conversional lines based on KAS and FWO model free methods, respectively. The apparent activation energy (E) values and linear correlation coefficient (R^2) are shown in Table 3; the linear correlation coefficients for getting the activation energy are in the range of 0.9783–0.9999 and the fitting is good for every linear plot. As shown in Table 3, the activation energy within α=0.15–0.85 was depicted in this study because of lower correlation values at conversion degrees below 0.15 and above 0.85.

The distribution of the activation energy for the propellant samples is presented in Fig. 7. The activation energy computed by KAS and FWO methods showed excellent agreement with each other, and only less than 5% deviation. This small deviation is attributed to the different approximations used in the algorithms [32, 36]. Several

authors reported that the results with deviations lower than 10% between two direct kinetic methods validated the reliability of the performed calculations and the excellent predictive power of the kinetic methods [32, 64]. Thus, the consistency of results from both methods, and the measured TG curves from multi-heating rate, validated the accuracy and reliability of the estimated activation energy. It is worth noting that the value of activation energy is commonly affected by several factors, such as different kinetics model, heating rate, sample nature, particle size and different types of thermal analysis technique. Therefore, the activation energy of our propellant samples is only valid for this kind of experimental parameters mentioned in sections 2.2 and 2.3.

Before the discussion of the activation energy distribution dependent on the conversion rate, it is worth noting that activation energy represents the minimum energy requirement for a reaction started, in other words, higher value of activation energy means slower reaction rate and more difficulty of a reaction starting. From an overall perspective of Fig. 7, the nonlinear relationship of the effective activation energy values with conversion rate at different stages (II and III) indicates that propellant samples are expected to be decomposed by multistep kinetics with complex reaction included parallel, competitive, consecutive and reversible reactions [35, 37, 43, 49, 56, 60].

The activation energy of the main decomposition of the HTPB propellant, corresponding to stage II in Fig. 7, is approximately 110–280 kJ mol^{-1} [30, 35, 37, 65, 66]. Lee [65] examined the thermal degradation of AP/HTPB/Al based propellant and demonstrated that its activation energy was about 163 kJ mol^{-1}. Celina et al. [66] revealed that the activation energy of the main decomposition of AP/HTPB/Al was ~120 kJ mol^{-1}. The average activation energy of CP-Baseline in our case was found to

be 135.52 kJ mol^{-1} for the KAS method and 138.68 kJ mol^{-1} for the FWO method. Our obtained apparent activation energy values are in accordance with the different values reported in the literature. Several phenomena occur during this stage (II). Firstly, dissociation and sublimation of AP take place and various reactions appeared quickly in the gas phase between NH_3 and $HClO_4$, forming O_2, N_2O, Cl_2, and H_2O as side products. These reactions occur on crystal defect (LTD) and in the lattice of the remaining crystal (HTD) [49]. Simultaneously, multi-stage binder decomposition and further attack on the polymer are caused by the highly oxidizing species of decomposition products of AP such as Cl_2O and ClO_2 [35]. In the next stage (III, Fig. 7), the average E value is 231.62 kJ mol^{-1} (KAS method) and 231.91 (FWO method) which is higher than that of the stage II, indicating that the residual polymeric binder needs higher temperature to burnout. Recently, El-Basuony et al. determined the activation energy of the second decomposition of HTPB- binder as 240 kJ mol^{-1} [60]. Vargeese investigated the thermal decomposition of AP/HTPB/Al propellant and showed that the activation energy of residual polymeric binder occurred at around 230 kJ mol^{-1} [35]. Both these values are in fair agreement with the activation energy determined in our case.

To get more insights into the effect of OXA coolant on the decomposition behavior of composite propellants, their kinetic curves, *E* against α, were plotted and shown in Fig. 7. Stages II and III were significantly influenced by OXA addition and it can been that the activation energies of stage II are brought up from 135.52 kJ mol^{-1} (KAS method) and 138.68 kJ mol^{-1} (FWO method) to 150.26 kJ mol^{-1} (KAS method) and 152.77 (FWO method) for the sample CP-OXA1, and to 157.37 kJ mol^{-1} (KAS method) and 159.54 (FWO method) for CP-OXA2. Similar trend was also found for the stage III showing the important effect of the OXA content as well. This behavior

445 can be assigned to the endothermic effect of OXA that altered and inhibited
446 simultaneously the decomposition of AP and the binder on the propellant surface. The
447 role of OXA is comparable to that of burning rate suppressants reported in the
448 literature, demonstrating its capacity as coolant [44].

449 Concerning ADA, the evolution of activation energy of the ADA-based
450 propellants vis. α is shown in Fig. 7. Stages II is apparently affected by ADA addition
451 and it can be seen that the activation energies are brought down from 135.52 kJ mol^{-1}
452 (KAS method) and 138.68 kJ mol^{-1} (FWO method) to 102.95 kJ mol^{-1} (KAS method)
453 and 107.69 (FWO method) for the sample CP-ADA1, and to 96.95 kJ mol^{-1} (KAS
454 method) and 101.71 (FWO method) for CP-ADA2. It should be noted that the
455 decomposition of perchloric acid and oxidation of ammonia during AP decomposition
456 generates heat and the sublimation proceeds with heat absorption. In the uncatalyzed
457 propellant samples the diffusion process is predominant as confirmed also by
458 Vargeese [35]; whereas the presence of ADA, that undergoes an exothermic
459 decomposition, would have supported their *in-situ* reactions. On the contrary, the
460 stage III will be inhibited as shown in Table 3 and Fig. 7, where an increase of the
461 activation energy is obtained. These results corroborate those reported above for the
462 thermal decomposition. Finally we can deduce that ADA plays a dual role; the first as
463 catalyst and the second as coolant. Furthermore, it was revealed in our previous work
464 that ADA decreases the burning rate and improves the combustion stability [8]. Thus
465 this coolant improves the catalytic behavior of the main decomposition and does not
466 sacrifice performance on one hand. On the other hand, it allows getting a stable
467 combustion.

468 **4. Conclusions**

The effect of burning rate suppressants (OXA and ADA) on the thermal behavior and decomposition kinetics of AP/HTPB-based aluminized solid rocket propellant system is investigated. The decomposition of the propellants was observed in two main stages, where it was significantly influenced by the nature and the amount of the coolant addition. The TG/DTA analyses indicate that OXA has a good inhibition effect on the tow-stage decomposition of propellant and associated kinetic parameters. The kinetic analysis results also indicate an increase in the activation energy values during the overall processes showing the effectiveness of cooling effect and demonstrating the action of this ballistic modifier on the condensed-gas-phases, where it acts endothermically on the AP and binder decompositions. In contrast, the thermal analyses of ADA-based propellants revealed that the ADA plays a double role. The first concerns a catalytic effect on the first stage of the decomposition of propellant owing to its exothermicity and acts principally on the decomposition of AP that consequently promotes the binder decomposition. The activation energy of this stage is shifted to lower values with respect to that of the CP-Baseline. The decomposition second stage, however, appeared to be inhibited, since the temperature shifted to higher values as well the activation energy. This latter behavior is attributed to the presence of the inert gases released by the ADA decomposition.

This study brings new insight in the effect of burning rate suppressants on the decomposition of composite propellants and suggests that these amide coolants could be used in other propellant formulations containing other oxidizers like ammonium dinitramide or other binders like glycidyl azide polymer, since the search of appropriate formulations with best properties remains actually a challenge to substitute the current employed formulations based on AP for environmental reasons.

Acknowledgments:

The authors thank Dr. Stefano Dossi, Dr. Marco Fassina and Mr. Giovani Colombo, SPLab, Dept. of Aerospace Science and Technology, Politecnico di Milano for the preparation of some propellant samples and for the commissioning of the TG/DTA apparatus.

References

1. DeLuca LT, Shimada T, Sinditskii VP, Calabro M. Chemical Rocket Propulsion: A Comprehensive Survey of Energetic Materials. Springer; 2017.

2. Sutton GP, Biblarz O. Rocket propulsion elements. John Wiley & Sons; 2017.

3. Kubota N. Propellants and explosives: thermochemical aspects of combustion. John Wiley & Sons; 2015.

4. Singh G. Recent advances on energetic materials. New York: Nova Scientific Publishers; 2015.

5. Mezroua A, Khimeche K, Lefebvre MH, Benziane M, Trache D. The influence of porosity of ammonium perchlorate (AP) on the thermomechanical and thermal properties of the AP/polyvinylchloride (PVC) composite propellants. J Therm Anal Calorim. 2014;116(1):279-86.

6. Trache D, Klapötke TM, Maiz L, Abd-Elghany M, DeLuca LT. Recent advances in new oxidizers for solid rocket propulsion. Green Chem. 2017;19(20):4711-36. doi:10.1039/C7GC01928A.

7. Dey A, Sikder AK, Talawar MB, Chottopadhyay S. Towards new directions in oxidizers/energetic fillers for composite propellants: an overview. Cent Eur J Energ Mater. 2015;12(2):377-99.

8. Trache D, Maggi F, Palmucci I, DeLuca LT, Khimeche K, Fassina M et al. Effect of amide-based compounds on the combustion characteristics of composite solid rocket propellants. Arab J Chem. 2015. doi:10.1016/j.arabjc.2015.11.016.

519 9. de la Fuente JL. Mesoporous copper oxide as a new combustion catalyst for
520 composite propellants. J Propul Power. 2013;29(2):293-8.
521 10. Klager K, Zimmerman G. Steady burning rate and affecting factors: Experimental
522 results. In: DeLuca L, Price E, Summerfield M, editors. Nonsteady Burning and
523 Combustion Stability of Solid Propellants. Washington: Progress in Astronautics and
524 Aeronautics; 1992. p. 59-109.
525 11. Mirzajani V, Farhadi K, Pourmortazavi SM. Catalytic effect of lead oxide nano-
526 and microparticles on thermal decomposition kinetics of energetic compositions
527 containing TEGDN/NC/DAG. J Therm Anal Calorim. 2018;131(2):937-48.
528 12. Ghorpade VG, Dey A, Jawale LS, Kotbagi AM, Kumar A, Gupta M. Study of
529 burn rate suppressants in AP-based composite propellants. Propell Explos Pyrot.
530 2010;35(1):53-6.
531 13. Ishitha K, Ramakrishna P. Studies on the role of iron oxide and copper chromite
532 in solid propellant combustion. Combust Flame. 2014;161(10):2717-28.
533 14. Parhi A, Mahesh V, Shaji A, Levin G, Abraham P, Srinivasan V. Challenges in
534 the development of a slow burning solid rocket booster. Aerosp Sci Technol.
535 2015;43:437-44.
536 15. Strunin VA, Fedorychev A, Gunin S, Klyuchnikov A, Milekhin YM, Manelis GB.
537 Two-zone model for combustion of a composite solid propellant with a coolant.
538 Combust Explos Shock Waves. 2010;46(3):315-24.
539 16. Dey A, Ghorpade VG, Kumar A, Gupta M. Biuret: a potential burning rate
540 suppressant in ammonium chlorate (VII) based composite propellants. Cent Eur J
541 Energ Mater. 2014;11(1):3-13.

17. Jawalkar S, Kurva R, Sundaramoorthy N, Dombe G, Singh PP, Bhattacharya B. Studies on high burning rate composite propellant formulations using TATB as pressure index suppressant. Cent Eur J Energ Mater. 2012;9(3):237-49.

18. Williams GK, Palopoli SF, Brill TB. Thermal decomposition of energetic materials 65. Conversion of insensitive explosives (NTO, ANTA) and related compounds to polymeric melon-like cyclic azine burn-rate suppressants. Combust Flame. 1994;98(3):197-204.

19. Talawar MB, Nair JK, Pundalik SM, Satpute RS, Venugopalan S. Diaminofurazan (DAF): Thermolysis and evaluation as ballistic modifier in double base propellant. J Hazard Mater. 2006;136(3):978-81.

20. Talawar MB, Makashir PS, Nair JK, Pundalik SM, Mukundan T, Asthana SN et al. Studies on diaminoglyoxime (DAG): Thermolysis and evaluation as ballistic modifier in double base propellant. J Hazard Mater. 2005;125(1):17-22.

21. Stoner Jr CE, Brill TB. Thermal decomposition of energetic materials 46. The formation of melamine-like cyclic azines as a mechanism for ballistic modification of composite propellants by DCD, DAG, and DAF. Combust Flame. 1991;83(3):302-8.

22. Zhang XD, Li JM, Yang RJ, Zhao XQ. Effect of Azodicarbonamide on the Properties of BAMO-THF/PSAN Propellants. J Beijing Inst Tech. 2010;30(5):603-7.

23. Yan Q-L, Zhao F-Q, Kuo KK, Zhang X-H, Zeman S, DeLuca LT. Catalytic effects of nano additives on decomposition and combustion of RDX-, HMX-, and AP-based energetic compositions. Prog Energy Combust Sci. 2016;57:75-136.

24. Vyazovkin S, Chrissafis K, Di Lorenzo ML, Koga N, Pijolat M, Roduit B et al. ICTAC Kinetics Committee recommendations for collecting experimental thermal analysis data for kinetic computations. Thermochim acta. 2014;590:1-23.

566 25. Vargeese AA, Muralidharan K, Krishnamurthy V. Kinetics of nano titanium
567 dioxide catalyzed thermal decomposition of ammonium nitrate and ammonium
568 nitrate-based composite solid propellant. Propell Explos Pyrot. 2015;40(2):260-6.
569 26. Trache D, Khimeche K. Study on the influence of ageing on thermal
570 decomposition of double□base propellants and prediction of their in□use time. Fire
571 Mater. 2013;37(4):328-36.
572 27. Trache D, Tarchoun AF. Stabilizers for nitrate ester-based energetic materials and
573 their mechanism of action: a state-of-the-art review. J Mater Sci. 2018;53(1):100-23.
574 doi:10.1007/s10853-017-1474-y.
575 28. Cho B-S, Kim J-S, Kang S-C, Noh S-T. Thermal decomposition kinetics of
576 ferrocene modified poly (epichlorohydrin-co-2-(methoxymethyl) oxirane) based
577 polyurethane networks. Thermochim acta. 2013;556:18-22.
578 29. Rocco J, Lima J, Frutuoso A, Iha K, Ionashiro M, Matos J et al. Thermal
579 degradation of a composite solid propellant examined by DSC. J Therm Anal
580 Calorim. 2004;75(2):551-7.
581 30. Rocco J, Lima J, Frutuoso A, Iha K, Ionashiro M, Matos J et al. TG studies of a
582 composite solid rocket propellant based on HTPB-binder. J Therm Anal Calorim.
583 2004;77(3):803-13.
584 31. Trache D. Comments on “thermal degradation behavior of hypochlorite-oxidized
585 starch nanocrystals under different oxidized levels”. Carbohydr Polym. 2016;151:535-
586 7.
587 32. Ma Z, Chen D, Gu J, Bao B, Zhang Q. Determination of pyrolysis characteristics
588 and kinetics of palm kernel shell using TGA–FTIR and model-free integral methods.
589 Energy Convers Manage. 2015;89:251-9.

590 33. Moukhina E. Determination of kinetic mechanisms for reactions measured with
591 thermoanalytical instruments. J Therm Anal Calorim. 2012;109(3):1203-14.
592 34. Trache D, Abdelaziz A, Siouani B. A simple and linear isoconversional method to
593 determine the pre-exponential factors and the mathematical reaction mechanism
594 functions. J Therm Anal Calorim. 2017;128(1):335-48.
595 35. Vargeese AA. A kinetic investigation on the mechanism and activity of copper
596 oxide nanorods on the thermal decomposition of propellants. Combust Flame.
597 2016;165:354-60.
598 36. Vyazovkin S, Burnham AK, Criado JM, Pérez-Maqueda LA, Popescu C,
599 Sbirrazzuoli N. ICTAC Kinetics Committee recommendations for performing kinetic
600 computations on thermal analysis data. Thermochim acta. 2011;520(1):1-19.
601 37. Babar Z-u-d, Malik AQ. An investigation of thermal decomposition kinetics of
602 nano zinc oxide catalyzed composite propellant. Combust Sci Technol.
603 2015;187(8):1295-315.
604 38. Kohga M, Handa S. Thermal decomposition behaviors and burning characteristics
605 of composite propellants prepared using combined ammonium
606 perchlorate/ammonium nitrate particles. J Energ Mater. 2017:1-18.
607 doi:10.1080/07370652.2017.1316794.
608 39. Rodríguez-Pesina M, García-Domínguez J, García-Hernández F, Flores-Vélez
609 LM, Domínguez O. The thermal decomposition of ammonium perchlorate-aluminum
610 propellants in presence of metallic zinc particles. Mater Sci Appl. 2017;8(06):436-47.
611 40. Pourmortazavi SM, Rahimi-Nasrabadi M, Rai H, Jabbarzadeh Y, Javidan A.
612 Effect of nanomaterials on thermal stability of 1, 3, 6, 8-tetranitro carbazole. Cent Eur
613 J Energ Mater. 2017;14(1):201-16. doi:10.22211/cejem/65140.

614 41. Abusaidi H, Ghaieni HR, Pourmortazavi SM, Motamed-Shariati SH. Effect of
615 nitro content on thermal stability and decomposition kinetics of nitro-HTPB. J Therm
616 Anal Calorim. 2016;124(2):935-41.
617 42. Chatragadda K, Vargeese AA. Synergistically catalysed pyrolysis of hydroxyl
618 terminated polybutadiene binder in composite propellants and burn rate enhancement
619 by free-standing CuO nanoparticles. Combust Flame. 2017;182:28-35.
620 43. Chaturvedi S, Dave PN, Patel NN. Thermal decomposition of AP/HTPB
621 propellants in presence of Zn nanoalloys. Appl Nanosci. 2015;5(1):93-8.
622 44. Sun Y-L, Li S-F, Ding D-H. Effect of ammonium oxalate/strontium carbonate on
623 the burning rate characteristics of composite propellants. J Therm Anal Calorim.
624 2006;86(2):497-503.
625 45. Yan Q-L, Zeman S, Elbeih A, Song Z-W, Málek J. The effect of crystal structure
626 on the thermal reactivity of CL-20 and its C4 bonded explosives (I): thermodynamic
627 properties and decomposition kinetics. J Therm Anal Calorim. 2013;112(2):823-36.
628 46. Liu S-E, Zhou W-L, Yan Q-L, Qi X-F, An T, Perez-Maqueda L et al. New
629 findings on thermal degradation properties of fluoropolymers. J Therm Anal Calorim.
630 2017;128(2):675-85.
631 47. Dubey R, Chawla M, Siril PF, Singh G. Bi-metallic nanocomposites of Mn with
632 very high catalytic activity for burning rate enhancement of composite solid
633 propellants. Thermochim acta. 2013;572:30-8.
634 48. Chaturvedi S, Dave PN. A review on the use of nanometals as catalysts for the
635 thermal decomposition of ammonium perchlorate. J Saudi Chem Soc.
636 2013;17(2):135-49.
637 49. Dey A, Athar J, Varma P, Prasant H, Sikder AK, Chattopadhyay S. Graphene-iron
638 oxide nanocomposite (GINC): an efficient catalyst for ammonium perchlorate (AP)

639 decomposition and burn rate enhancer for AP based composite propellant. RSC Adv.
640 2015;5(3):1950-60.
641 50. Doyle C. Kinetic analysis of thermogravimetric data. J Appl Polym Sci.
642 1961;5(15):285-92.
643 51. Coats A, Redfern J. Kinetic parameters from thermogravimetric data. Nature.
644 1964;201(4914):68-9.
645 52. Trache D. Comments on “Effect of hydrolysed cellulose nanowhiskers on
646 properties of montmorillonite/polylactic acid nanocomposites” By Reza Arjmandi et
647 al. Int J Biol Macromolec. 2016(88):497-8.
648 53. Senum G, Yang R. Rational approximations of the integral of the Arrhenius
649 function. J Therm Anal. 1977;11(3):445-7.
650 54. Wu Z, Yang W, Tian X, Yang B. Synergistic effects from co-pyrolysis of low-
651 rank coal and model components of microalgae biomass. Energy Convers Manage.
652 2017;135:212-25.
653 55. Sell T, Vyazovkin S, Wight CA. Thermal decomposition kinetics of PBAN-binder
654 and composite solid rocket propellants. Combust Flame. 1999;119(1):174-81.
655 56. Wang Y-h, Liu L-l, Xiao L-y, Wang Z-x. Thermal decomposition of HTPB/AP
656 and HTPB/HMX mixtures with low content of oxidizer. J Therm Anal Calorim.
657 2015;119(3):1673-8.
658 57. Zhang W, Li P, Xu H, Sun R, Qing P, Zhang Y. Thermal decomposition of
659 ammonium perchlorate in the presence of Al (OH) 3· Cr (OH) 3 nanoparticles. J
660 Hazard Mater. 2014;268:273-80.
661 58. Zhu Y-L, Huang H, Ren H, Jiao Q-J. Effects of aluminum nanoparticles on
662 thermal decomposition of ammonium perchlorate. J Korean Chem Soc. 2013;57:109-
663 14.

664 59. Trunov MA, Umbrajkar SM, Schoenitz M, Mang JT, Dreizin EL. Oxidation and
665 melting of aluminum nanopowders. J Phys Chem B. 2006;110(26):13094-9.
666 60. El-Basuony SA, Sadek MA, Wafy TZ, Mostafa HE. Thermokinetic studies of
667 polyurethanes based on hydroxyl-terminated polybutadiene prepolymer. J Therm
668 Anal Calorim. 2017:1-7. doi:10.1007/s10973-017-6552-5.
669 61. Patil PR, Krishnamurthy VeN, Joshi SS. Differential scanning calorimetric study
670 of HTPB based composite propellants in presence of nano ferric oxide. Propell Explos
671 Pyrot. 2006;31(6):442-6.
672 62. Gaurav M, Ramakrishna P. Effect of mechanical activation of high specific
673 surface area aluminium with PTFE on composite solid propellant. Combust Flame.
674 2016;166:203-15.
675 63. Hanson-Parr DM, Parr TP. Thermal properties measurements of solid rocket
676 propellant oxidizers and binder materials as a function of temperature. J Energ Mater.
677 1999;17(1):1-48.
678 64. Jiang L, Yuan X, Li H, Xiao Z, Liang J, Wang H et al. Pyrolysis and combustion
679 kinetics of sludge–camphor pellet thermal decomposition using thermogravimetric
680 analysis. Energy Convers Manage. 2015;106:282-9.
681 65. Lee I, editor. Thermal response of AP and aluminized AP/HTPB-based
682 propellants with varying composition. 35th AIAA/ASME/SAE/ASEE Joint
683 Propulsion Conference and Exhibit 1999; Los Angeles, Califormia.
684 66. Celina M, Minier L, Assink R. Development and application of tools to
685 characterize the oxidative degradation of AP/HTPB/Al propellants in a propellant
686 reliability study. Thermochim acta. 2002;384(1):343-9.

687

688

689 **List of Figures**

702

703

Tables

Table 1

Mass fraction of the investigated propellant formulations.

Propellant	fAP	cAP + Coolant	HTPB	Al	Coolant (% of cAP)	
					OXA	ADA
CP-Baseline	10	58	14	18	–	–
CP-OXA1	10	58	14	18	0.5	–
CP-OXA2	10	58	14	18	3	–
CP-ADA1	10	58	14	18	–	0.5
CP-ADA2	10	58	14	18	–	3

Table 2

Sample	Heating rate	Stage II			Stage III		
	°C min^{-1}	T_i /°C	T_p /°C	Mass loss /%	T_i /°C	T_p /°C	Mass loss /%
CP-Baseline	5	288.2	352.6	72.14	421.3	441.6	9.09
	10	299.1	371.2	72.54	426.4	454.9	4.55
	15	303.8	379.5	70.73	443.1	460.8	3.90
	20	306.8	386.8	73.21	444.9	466.7	4.74
	25	321.1	389.8	74.70	448.2	471.4	5.32
CP-OXA1	5	291.4	359.1	73.26	423.0	449.2	5.78
	10	303.1	369.8	73.64	428.7	458.6	7.80
	15	311.8	382.9	73.73	445.1	466.7	4.33
	20	321.9	385.3	74.06	449.7	469.8	5.05
	25	326.8	394.1	74.52	453.9	476.3	5.20
CP-OXA2	5	309.9	361.2	72.66	425.0	452.0	6.60
	10	313.4	371.9	73.37	434.4	463.8	5.29
	15	324.5	392.1	72.70	449.2	468.1	5.20
	20	328.0	393.4	76.57	453.6	472.4	5.62
	25	331.3	401.9	75.71	457.5	478.2	4.00
CP-AZO1	5	283.4	344.7	70.23	420.1	448.0	7.13
	10	294.4	368.5	71.52	424.2	457.8	5.02
	15	301.7	382.6	73.62	440.2	464.9	4.02
	20	305.9	384.5	73.68	442.5	469.4	4.31
	25	311.3	390.1	74.36	445.8	476.1	3.01
CP-AZO2	5	282.5	333.9	70.03	417.3	451.1	8.61
	10	290.9	355.7	71.16	431.2	462.8	6.03
	15	294.9	372.8	69.49	435.9	466.0	7.63
	20	302.5	377.1	74.21	438.2	470.4	6.24
	25	306.1	384.0	76.57	441.6	477.1	8.28

T_i: initial temperature of decomposition (°C); T_p: peak temperature of decomposition (°C).

719 **Table 3**

Sample	A	Stage II				Stage III			
		KAS method		FWO method		KAS method		FWO method	
		E /kJ mol^{-1}	R^2	E /kJ mol^{-1}	R^2	E /kJ mol^{-1}	R^2	E /kJ mol^{-1}	R^2
CP-Baseline	0.15	147.46	0.9958	149.41	0.9963	238.76	0.9902	238.31	0.9910
	0.25	140.05	0.9899	142.75	0.9914	230.27	0.9986	230.36	0.9988
	0.35	144.96	0.9876	147.51	0.9892	242.78	0.9989	242.34	0.9990
	0.45	121.32	0.9847	125.20	0.9871	237.74	0.9988	237.64	0.9989
	0.55	120.17	0.9829	124.23	0.9856	218.82	0.9924	219.77	0.9932
	0.65	129.22	0.9989	132.86	0.9991	220.44	0.9830	221.44	0.9848
	0.75	135.48	0.9948	138.92	0.9955	226.40	0.9839	227.25	0.9856
	0.85	145.46	0.9967	148.54	0.9971	237.73	0.9873	238.17	0.9885
	Average	135.52		138.68		231.62		231.91	
CP-OXA1	0.15	149.13	0.9892	151.18	0.9906	246.95	0.9964	246.22	0.9967
	0.25	150.45	0.9865	152.65	0.9881	255.51	0.9922	254.44	0.9929
	0.35	151.70	0.9864	153.99	0.9880	253.76	0.9849	252.87	0.9863
	0.45	152.19	0.9783	154.59	0.9810	270.68	0.9971	269.04	0.9973
	0.55	150.38	0.9841	152.98	0.9861	253.62	0.9958	252.91	0.9961
	0.65	150.57	0.9811	153.25	0.9835	252.07	0.9814	251.54	0.9831
	0.75	148.83	0.9861	151.69	0.9879	266.68	0.9982	265.54	0.9984
	0.85	148.84	0.9841	151.80	0.9863	263.03	0.9977	262.15	0.9979
	Average	150.26		152.77		257.79		256.84	
CP-OXA2	0.15	157.29	0.9912	158.96	0.9922	335.39	0.9960	330.30	0.9963
	0.25	158.39	0.9932	160.21	0.9940	277.46	0.9937	275.33	0.9943
	0.35	160.52	0.9904	162.40	0.9915	275.50	0.9980	273.55	0.9982
	0.45	155.61	0.9811	157.85	0.9834	282.22	0.9979	280.03	0.9981
	0.55	158.29	0.9861	160.52	0.9878	277.26	0.9840	275.44	0.9853
	0.65	157.42	0.9819	159.79	0.9841	292.59	0.9924	290.12	0.9930

	0.75	155.71	0.9873	158.26	0.9889	289.73	0.9987	287.50	0.9988
	0.85	155.69	0.9850	158.33	0.9870	284.50	0.9981	282.62	0.9983
	Average	157.37		159.54		289.33		286.86	
CP-AZO1	0.15	110.19	0.9953	114.07	0.9961	242.53	0.9908	242.01	0.9917
	0.25	110.04	0.9941	114.12	0.9952	250.16	0.9933	249.35	0.9939
	0.35	107.14	0.9920	111.52	0.9934	250.23	0.9823	249.50	0.9839
	0.45	103.29	0.9905	107.99	0.9922	270.54	0.9946	268.88	0.9950
	0.55	100.00	0.9906	104.99	0.9924	259.45	0.9811	258.43	0.9827
	0.65	98.27	0.9912	103.45	0.9929	249.84	0.9834	249.39	0.9849
	0.75	97.35	0.9903	102.67	0.9921	266.99	0.9985	265.80	0.9987
	0.85	97.33	0.9839	102.75	0.9869	265.03	0.9977	264.03	0.9979
	Average	102.95		107.69		256.85		255.92	
CP-AZO2	0.15	103.38	0.9969	107.49	0.9974	280.55	0.9936	278.16	0.9941
	0.25	99.17	0.9998	103.56	0.9998	279.88	0.9868	277.62	0.9874
	0.35	97.87	0.9959	102.41	0.9967	273.11	0.9970	271.25	0.9972
	0.45	94.03	0.9946	98.88	0.9956	284.81	0.9918	282.48	0.9924
	0.55	88.89	0.9989	94.11	0.9991	285.21	0.9811	282.97	0.9826
	0.65	96.90	0.9987	101.84	0.9990	290.76	0.9930	288.35	0.9936
	0.75	96.34	0.9905	101.38	0.9921	322.22	0.9956	318.36	0.9959
	0.85	99.00	0.9971	104.04	0.9977	296.34	0.9999	293.86	0.9999
	Average	96.95		101.71		289.11		286.63	

720

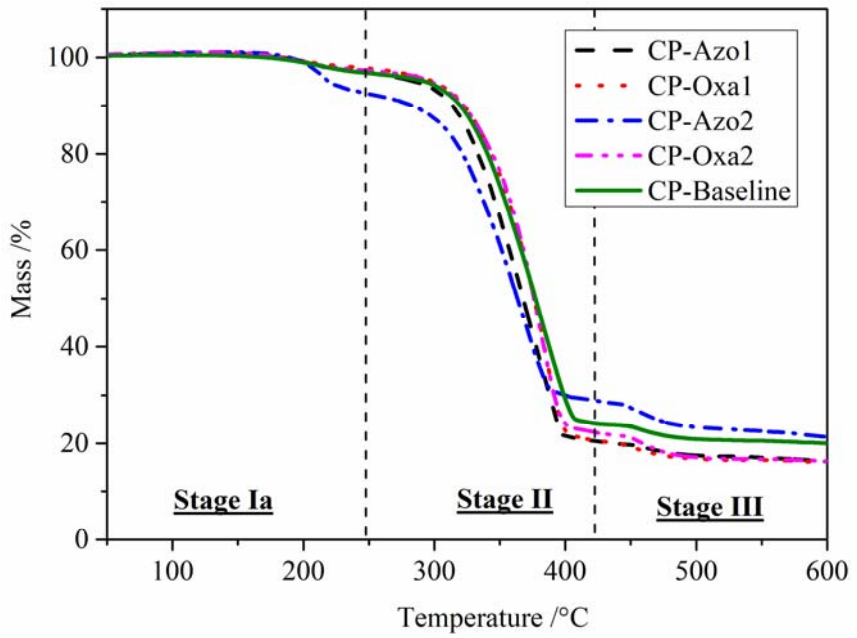
Mass /%
Temperature /°C
CP-Azo1
CP-Oxa1
CP-Azo2
CP-Oxa2
CP-Baseline
Stage Ia
Stage II
Stage III

(a)

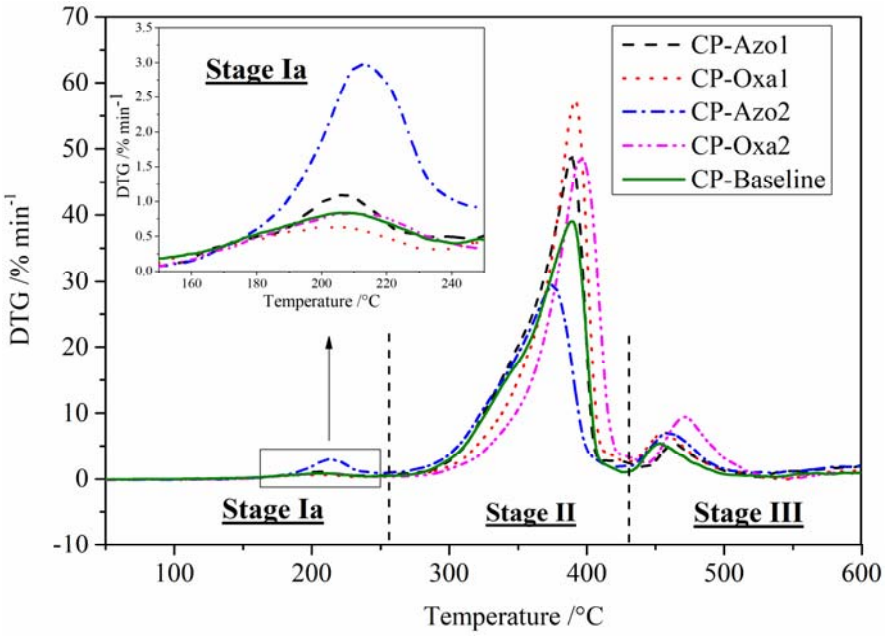
DTG /% min-1
Temperature /°C
CP-Azo1
CP-Oxa1
CP-Azo2
CP-Oxa2
CP-Baseline
Stage Ia
Stage II
Stage III

(b)

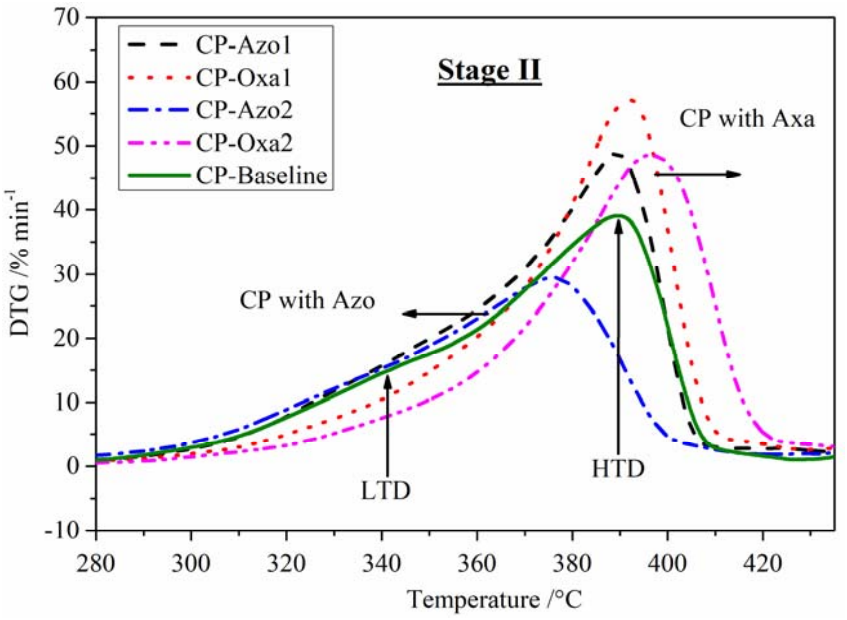
CP-Azo1
CP-Oxa1
CP-Azo2
CP-Oxa2
CP-Baseline
Stage II
CP with Axa
CP with Azo
LTD
HTD
DTG /% min-1
Temperature /°C

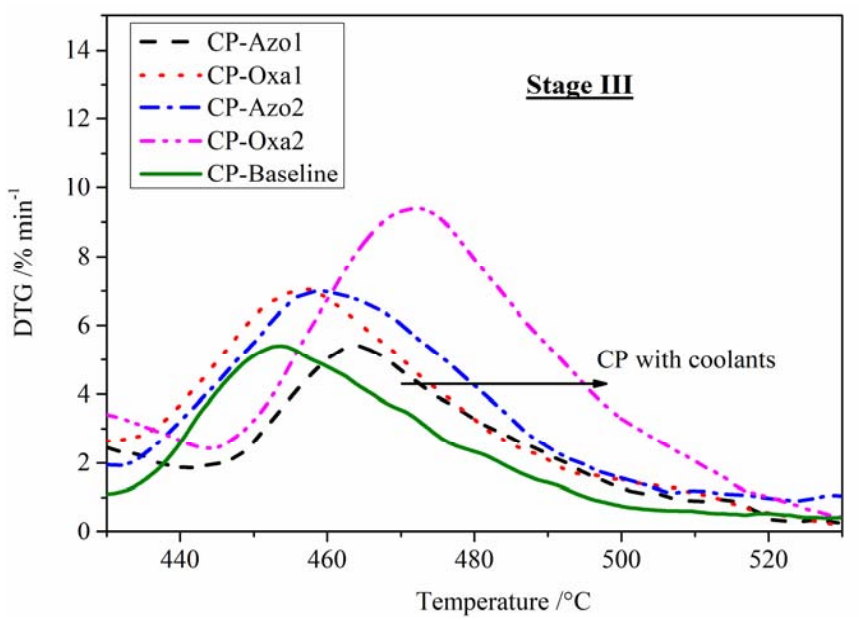
CP-Azo1
CP-Oxa1
CP-Azo2
CP-Oxa2
CP-Baseline
Stage III
CP with coolants
DTG /% min-1
Temperature /°C

(c) **(d)**

Fig.1

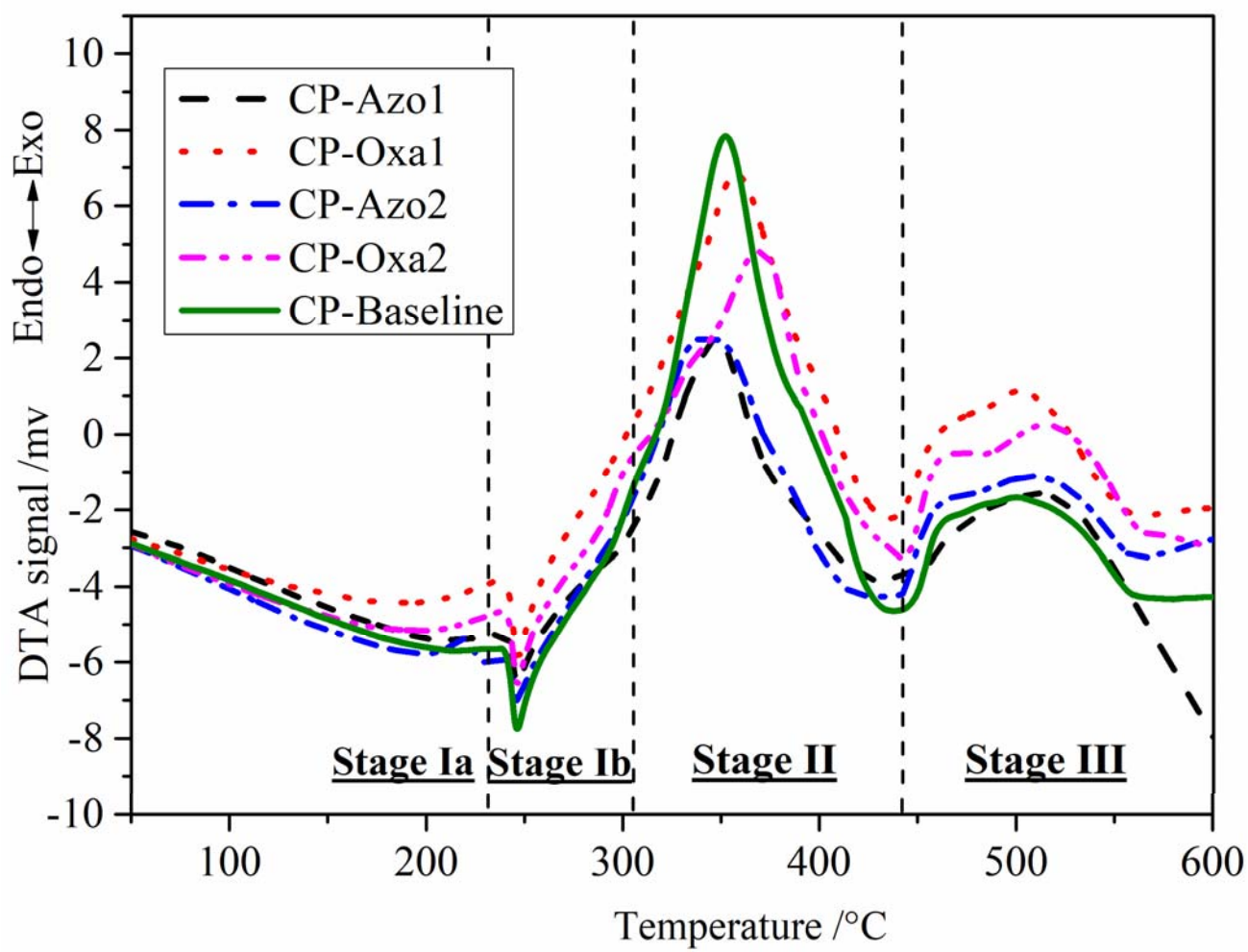
CP-Azo1
CP-Oxa1
CP-Azo2
CP-Oxa2
CP-Baseline
Endo→Exo
DTA signal /mv
Temperature /°C
Stage Ia
Stage Ib
Stage II
Stage III
10
8
6
4
2
0
-2
-4
-6
-8
-10
100
200
300
400
500
600

Fig.2.

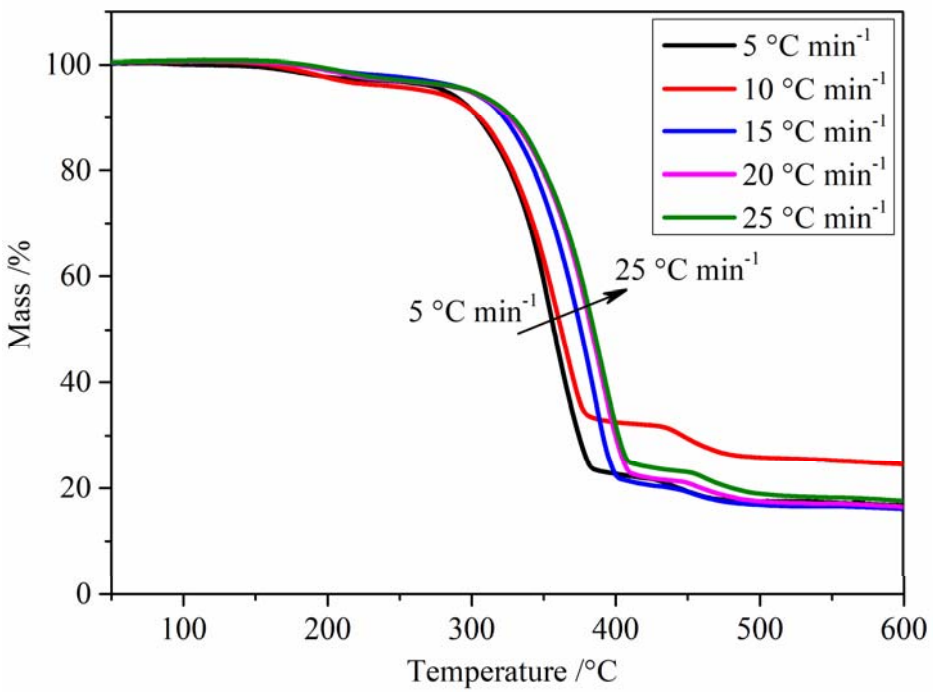
5 °C min-1
10 °C min-1
15 °C min-1
20 °C min-1
25 °C min-1
Mass /%
Temperature /°C
5 °C min-1
25 °C min-1

(a)

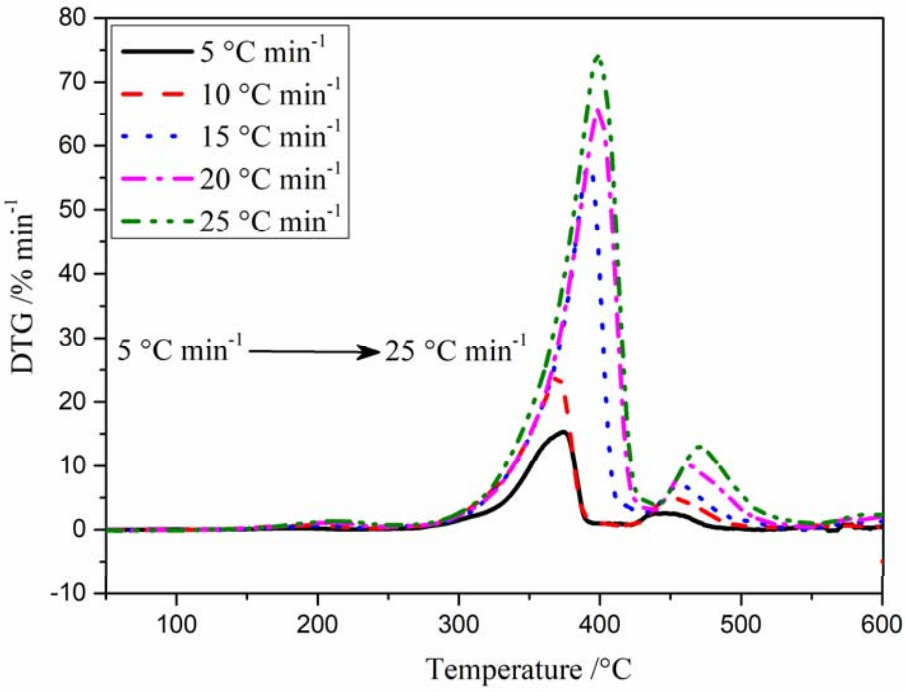
5 °C min-1
10 °C min-1
15 °C min-1
20 °C min-1
25 °C min-1
DTG /% min-1
Temperature /°C
5 °C min-1
25 °C min-1

(b)

Fig.3

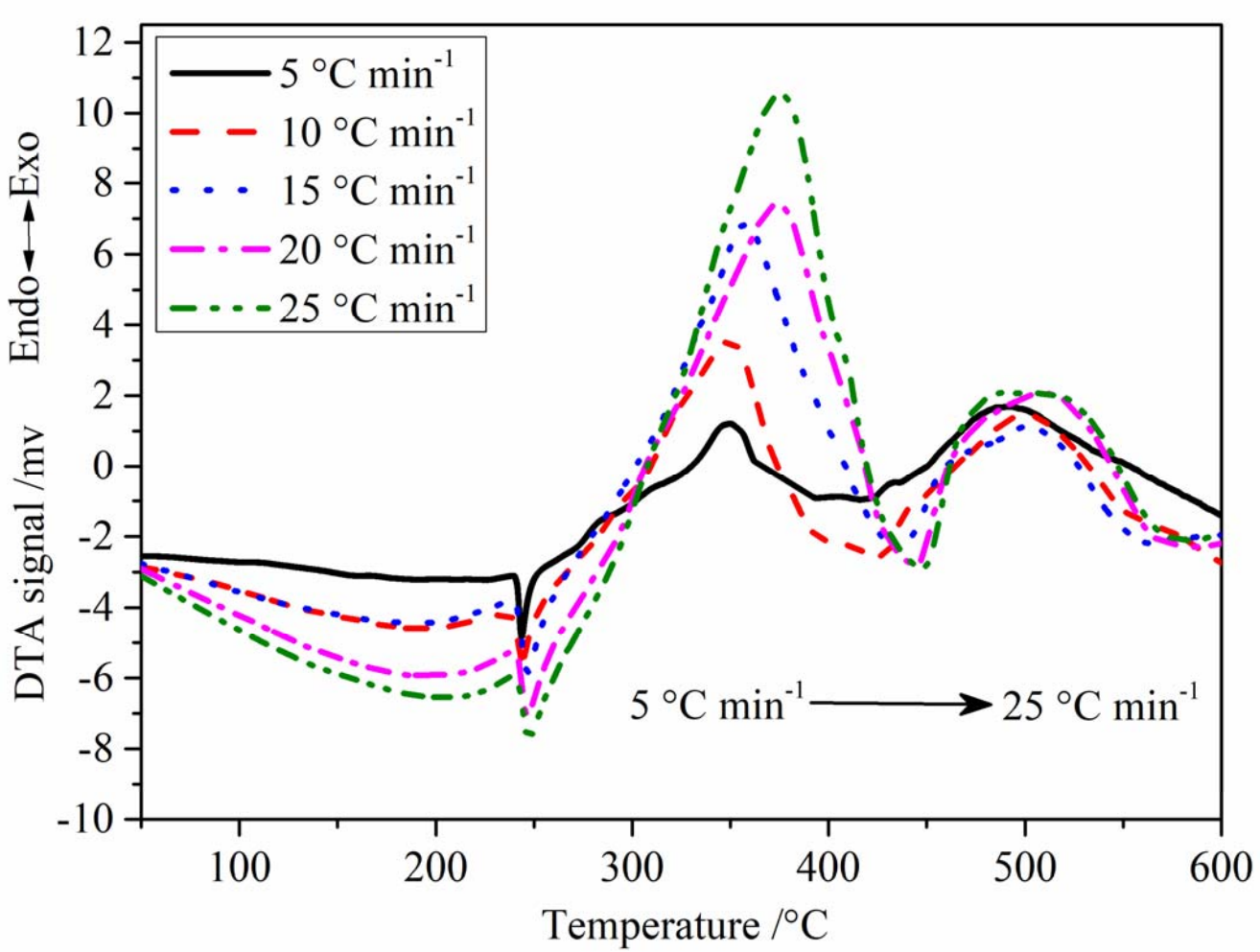
5 °C min-1
10 °C min-1
15 °C min-1
20 °C min-1
25 °C min-1
Endo⟷Exo
DTA signal /mv
Temperature /°C
5 °C min-1 ⟶ 25 °C min-1
12
10
8
6
4
2
0
-2
-4
-6
-8
-10
100
200
300
400
500
600

Fig.4.

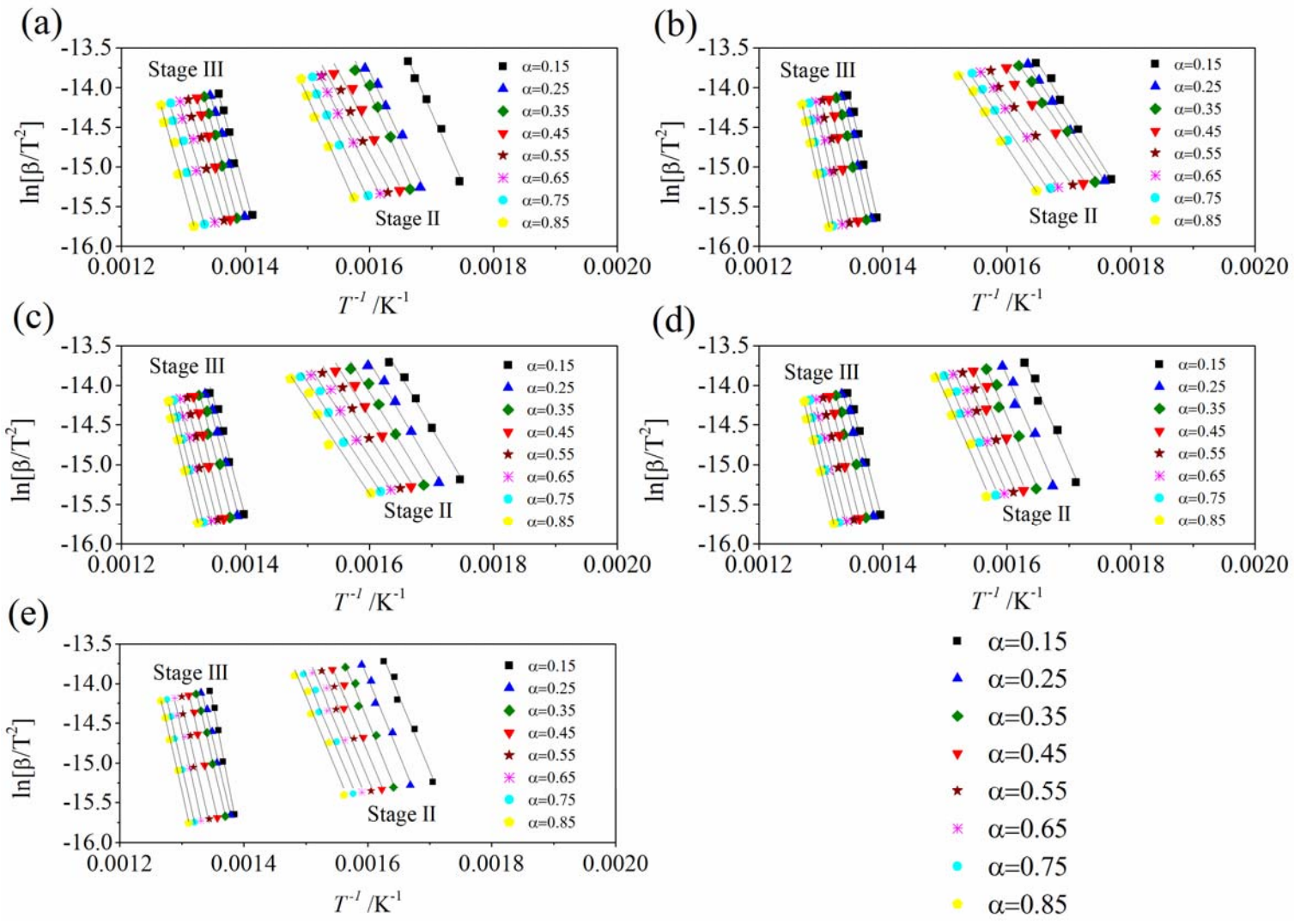
(a)
(b)
(c)
(d)
(e)
Stage III
Stage II
ln[β/T²]
T⁻¹ /K⁻¹
-13.5
-14.0
-14.5
-15.0
-15.5
-16.0
0.0012
0.0014
0.0016
0.0018
0.0020
α=0.15
α=0.25
α=0.35
α=0.45
α=0.55
α=0.65
α=0.75
α=0.85

17

18 **Fig.5.**

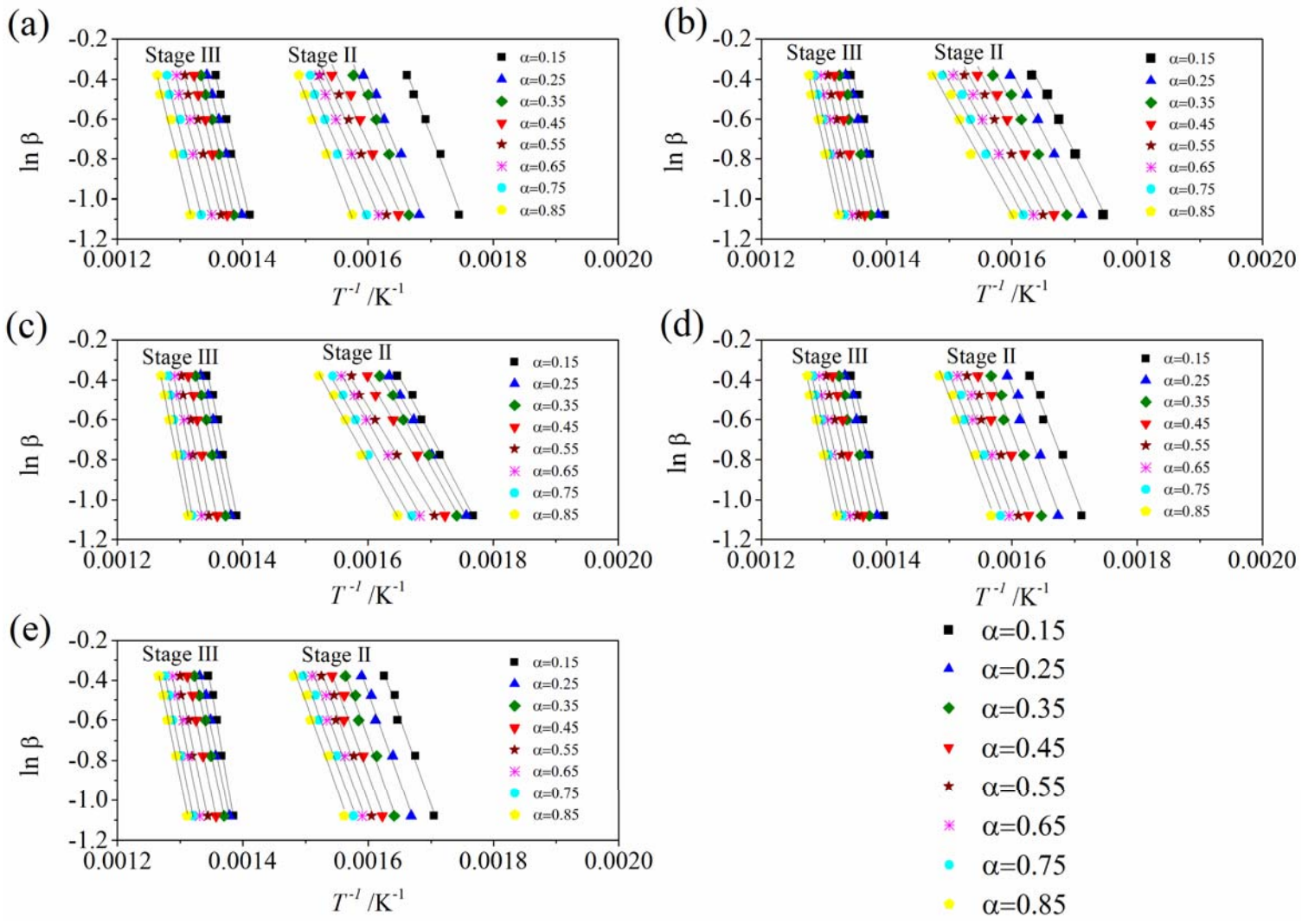
(a)
(b)
(c)
(d)
(e)
Stage III
Stage II
ln β
T^{-1} /K^{-1}
-0.2
-0.4
-0.6
-0.8
-1.0
-1.2
0.0012
0.0014
0.0016
0.0018
0.0020
α=0.15
α=0.25
α=0.35
α=0.45
α=0.55
α=0.65
α=0.75
α=0.85

19

20 **Fig.6.**

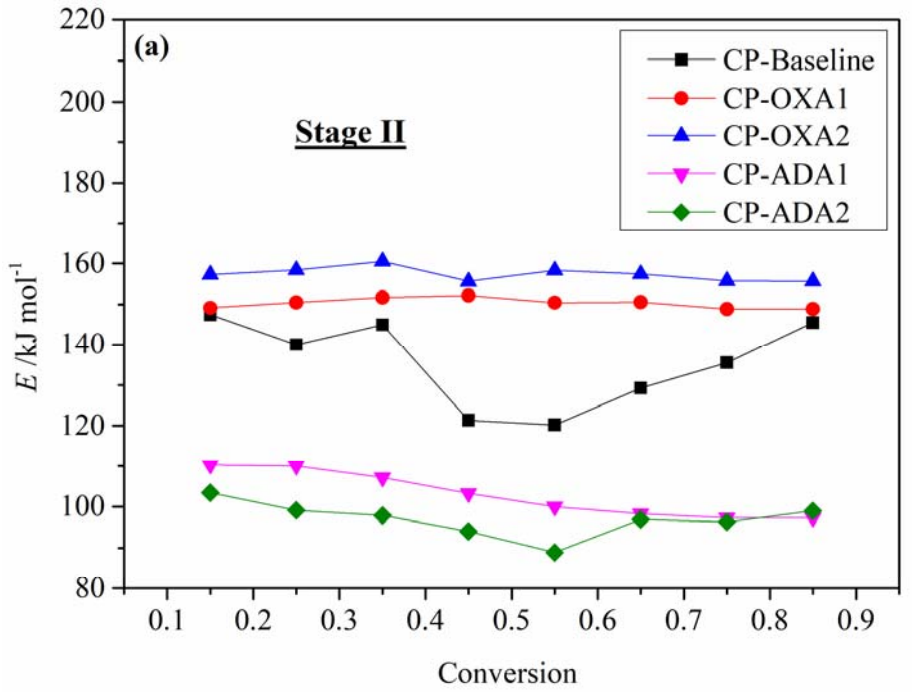
(a)
Stage II
CP-Baseline
CP-OXA1
CP-OXA2
CP-ADA1
CP-ADA2
E /kJ mol-1
Conversion
220
200
180
160
140
120
100
80
0.1
0.2
0.3
0.4
0.5
0.6
0.7
0.8
0.9

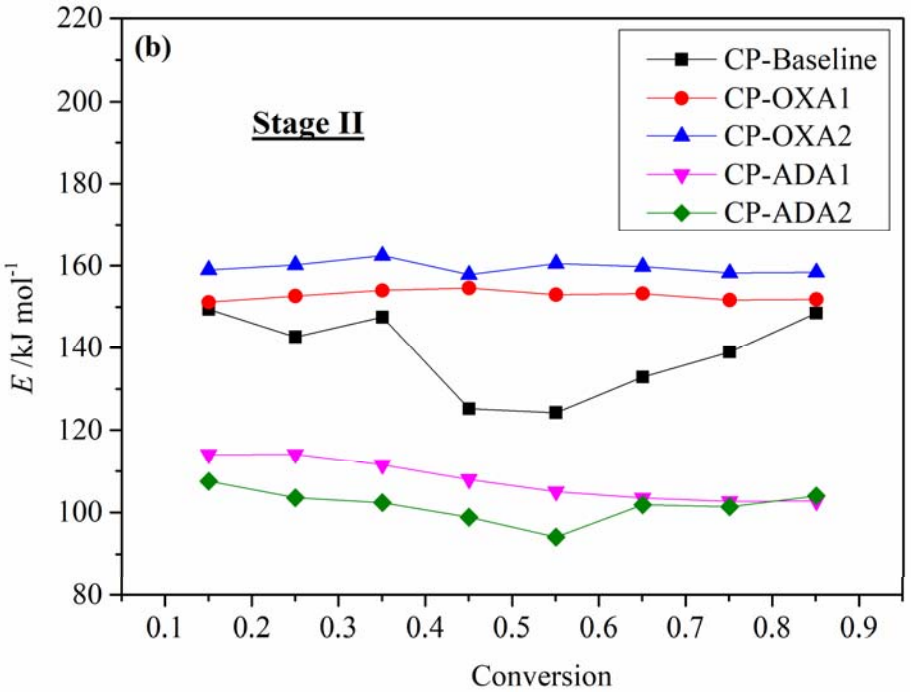
(b)
Stage II
CP-Baseline
CP-OXA1
CP-OXA2
CP-ADA1
CP-ADA2
E /kJ mol-1
Conversion
220
200
180
160
140
120
100
80
0.1
0.2
0.3
0.4
0.5
0.6
0.7
0.8
0.9

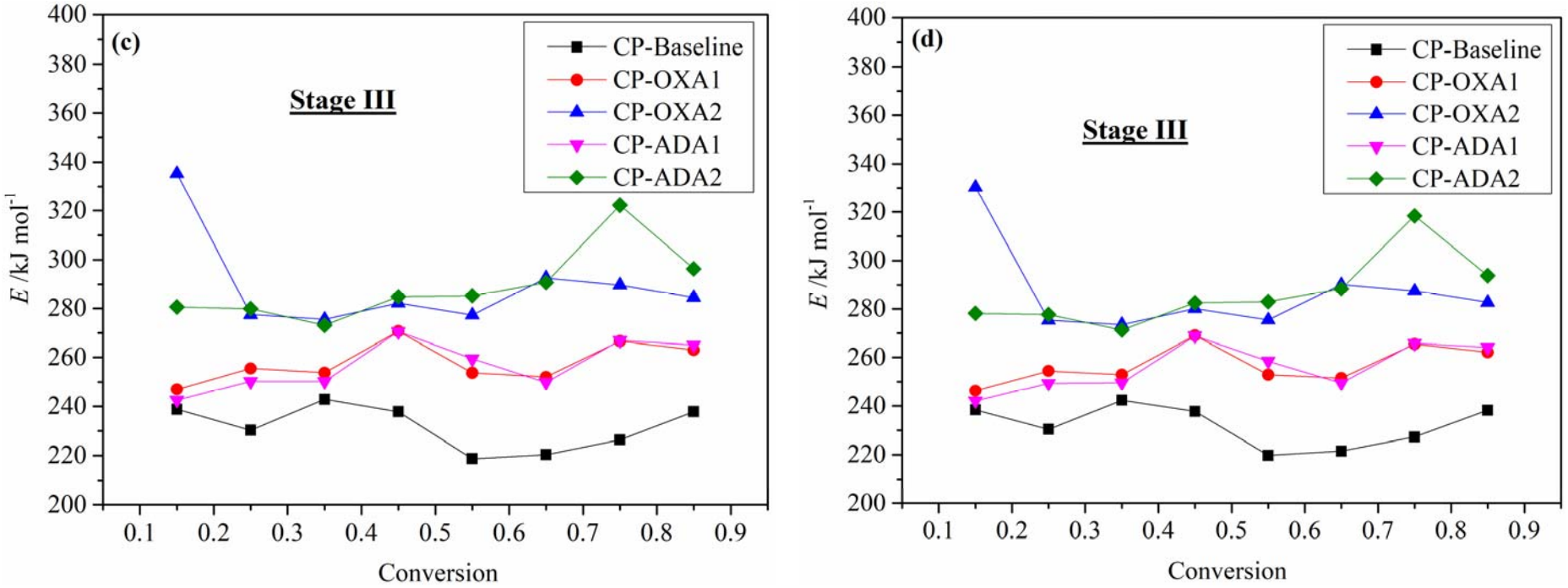
(c)
Stage III
CP-Baseline
CP-OXA1
CP-OXA2
CP-ADA1
CP-ADA2
E /kJ mol-1
Conversion
(d)
Stage III
CP-Baseline
CP-OXA1
CP-OXA2
CP-ADA1
CP-ADA2
E /kJ mol-1
Conversion

Fig.7.